J Mater Sci (2013) 48:4866–4875
DOI 10.1007/s10853-013-7265-1

Measurement of thermal diffusivity for alumina borosilicate glass bearing TRISO fuel particles: experiment and modelling correlation

Klaudio Bari · Sohaib Z. Khan · Tristan Lowe · Johar K. Farooqi

Received: 30 November 2012 / Accepted: 21 February 2013 / Published online: 6 March 2013

Abstract A long-term disposal of a nuclear waste package requires a matrix material that possesses a high thermal conductivity in order to release the decay heat from the fission products. In this study, the thermal diffusivity (α) of alumina borosilicate glass (ABG), encapsulating surrogated tristructural-isotropic (TRISO) particles, has been measured experimentally using the laser flash analysis (LFA) methodology. Image-based models were developed using X-ray computed tomography for glass samples bearing different proportions of TRISO particles. Simpleware software generated finite element (FE) models which then were solved using Abaqus software. The matrices were examined at different waste loadings (10, 20 and 30 wt%) at a temperature of 50 °C. The modelling results were in close agreement with the experimental results and the deviations were within the bounds of standard numerical error (<5 %). The thermal diffusivity of the samples was increased with increasing proportion of TRISO particles. For the maximum mechanically stable matrix, the thermal diffusivity was found to be $0.92 \pm 0.021 \times 10^{-6}$ and 0.94×10^{-6} m^2 s^{-1} measured by LFA and modelling, respectively.

K. Bari (✉)
School of Mechanical, Aerospace and Civil Engineering (MACE), University of Manchester, Pariser Building, Manchester M60 1QD, UK
e-mail: klaudiobari@icloud.com

S. Z. Khan
National University of Sciences and Technology (Islamabad), PNEC, PNS Jauhar, Habib Rehmatullah Road, Karachi, Pakistan

T. Lowe
Material Science Center, Henry Moseley Facilities, University of Manchester, Manchester M1 7HS, UK

J. K. Farooqi
DHA Suffa University, DG-78, DHA Phase VII Ext., Karachi 75500, Pakistan

Introduction

The thermal diffusivity of alumina borosilicate glass (ABG) bearing TRISO particles plays an important role in estimation of dissipation of radioactive waste heat. The particles were chosen to have SiC outer layer in order to provide chemical compatibility with ABG [1]. SiC layer has the highest thermal conductivity (168 W m^{-1} K^{-1}) in TRISO particles [2]. This reduces the probability of forming a hot spot in the waste form. As the glass matrix was only recently developed, there were no investigations and/or calculations done for the thermal diffusivity of a glass bearing TRISO particles. However, many studies were directed towards measuring the thermal diffusivity and conductivity of glass and TRISO particles independently. In a previous study, the thermal conductivities of TRISO layers were measured using time-domain thermoreflectance and they are listed in Table 1 [2]. The waste loading (proportion of TRISO particles in the matrix) may play an important role in the heat conduction. Therefore, in this study, the tests were conducted on three specimens bearing different proportions of TRISO particles.

Previous research measured the heat conduction of carbon fibre-reinforced lithia silicate glass ($Li_2O{\cdot}2Al_2O_3{\cdot}6SiO_2$). The purpose of that study was to establish some of the variables which affect the conduction of heat in a composite, having a different orientation of carbon fibre-reinforced lithia alumina silicate glass [3]. The thermal conductivity of the composite (30 W m^{-1} K^{-1}) was estimated by measuring the thermal diffusivity (α) in the

Table 1 Thermal conductivity, density, and specific heat of different layers of TRISO particle [2]

Material	Thermal conductivity, k (W m^{-1} K^{-1})	Density, ρ (kg m^{-3})	Specific heat, C_p (kJ kg^{-1} K^{-1})
ZrO_2	2.5	5700	0.21
Buffer	5.8	1150	0.71
IPyC	13.5	1850	0.71
SiC	168	3200	0.89

parallel direction to the carbon fibres' plane, using laser flash analyses (LFA) as described in Eq. 1. The thermal conductivity (k) of the lithia alumina silicate glass without carbon fibres was estimated to be around 1.6 W m^{-1} K^{-1}.

$$k = \alpha \cdot \rho \cdot C_p \tag{1}$$

ρ Density (kg m^{-3})
C_p Heat capacity (J kg^{-1} K^{-1})
α Thermal diffusivity (m^2 s^{-1})

In this study, LFA was used as a direct method for measuring off-axis thermal diffusivity. This methodology was initially developed by Parker et al. [4]. The front face of a disc-shaped specimen was exposed to a short pulse of laser beam and the thermal diffusivity of the specimen was determined by measuring the temperature as function of time from the rear face. The thermal diffusivity (α) was calculated by the given Eq. 2:

$$\alpha = \frac{0.1388L^2}{t_{1/2}} \tag{2}$$

L Thickness of the sample (m)
$t_{1/2}$ Time required to reach one half of the maximum temperature on the rear face (s)

The ZrO_2 kernel was chosen to simulate UO_2 fuel kernel of TRISO particle; its diameter was 500 μm and it was surrounded by several consecutive spherical layers. Each layer of a TRISO particle is separate, designed to have a specific function in the fuel performance and retention of fission products, and therefore each layer has a specific thermal conductivity. A porous pyrolytic carbon buffer layer provides a void volume for gaseous fission products and accommodates the fuel kernel's swelling that occurs due to its fission. An internal pyrolytic carbon (IPyC) reduces tensile stress on SiC and acts as a diffusion barrier to metallic fission products. A silicon carbide layer (SiC) ensures leak tightness to metallic fission products during normal and accidental scenarios. An outer pyrolytic carbon (OPyC) also reduces tensile stress on SiC and provides bonding surface for the graphite compact. OPyC was not coated in this study due to its thermal oxidation with glass during hot-isostatic sintering [5]. The aim of the research was to investigate the thermal properties of a waste form containing TRISO particles with SiC as an outer layer. The spent fuel particles are generated at a particular stage of the waste management process, namely acidic intercalation of a graphite compact. The intercalation of TRISO particles from the graphite compact is essential to separate high-level waste (TRISO particles) from the intermediate-level waste (irradiated graphite). In order to oblige an appropriate conditioning and disposal route in the geological repository, a previous study proposed the elimination of OPyC by thermal oxidation [6]. It prevents the appearance of thermal cracks in the glass matrix during rapid cooling; thus, SiC becomes the outer layer.

It is important to know that high-level waste (in this case, spent TRISO particles) generates decay heat after disposal. Since a repository serves as a thermal insulator, the heat generated by the waste form causes an increase in the temperature (90–250 °C). The equilibrium temperature of a waste form in the canister has been shown as a function of the canister dimension, host rock thermal conductivity, waste loading percentage and post-burial time [7].

When dealing with heat-generating nuclear waste, a majority of the consideration must be given to the thermal loading of an emplacement cell in a borehole and the waste package thermal conductivity. For example, the temperature of the waste package in the Yucca mountain repository was designed to be within 200 °C [8].

Key parameters of a layout configuration in the repository design are the thermal loading and cooling performance. Thermal loading, resulting from a designed repository, depends mainly on heat generation of the waste package, thermal properties of the host rock, spacing between the waste packages and quality of the thermal interface between the waste package and the host rock [9]. For waste packages with high thermal conductivity, the cell diameter may be large and may contain a high waste loading, thus providing a more compact disposal area. If the thermal conductivity is too low and heat generation is too high, damage may occur to the waste package due to an extreme rise in temperature [10]. The present research is an effort to validate the values of thermal diffusivity, obtained from the experimental work (LFA), through simulation using image-based modelling (IBM).

The experimental thermal diffusivity was validated through IBM. The IBM methodology started by acquiring X-ray computed tomography (CT) images that were then converted into digital 3D geometry. The resulting 3D model was a set of segmented masks, labelled according to the greyscale intensities. For the purpose of finite element (FE) analysis, Simpleware software was used to generate a

mixture of tetrahedral and hexahedral geometric elements that were represented by both TRISO particle layers and glass matrix. Next, Abaqus/CAE software was used to solve the FE model by simulating parameters similar to the ones that were used in the LFA.

This article also discusses deviations between the thermal diffusivity measured experimentally (LFA) and its values measured through modelling (Abaqus software).

Experimental procedure

Material

The thermal conductivities of TRISO particles layers are listed in Table 1; these were used in the material properties section of Abaqus software. The values were measured using time-domain thermoreflectance [2]. The thermal conductivity of the layers depends on their deposition temperatures and gas precursor ratios during the chemical vapour deposition (CVD) that was used to coat the particles.

TRISO particles, having a ZrO_2 kernel (diameter 500 μm), were coated using the fluidized bed chemical vapour deposition (FBCVD) process. This mechanism consisted of a 200-mm-long graphite tube (35 mm inner diameter) equipped with a multi-hole nozzle as a gas distributer installed inside a furnace. The furnace was heated by resistance graphite elements and cooled externally with water. The parameters and precursors are described by Kercher et al. [11]. The layers were coated according to the following layer thickness: TRISO particles: ZrO_2 kernel/buffer carbon 90 μm/IPYC 60 μm/SiC 60 μm.

Glass powder of grain size less than 1 μm was used as an initial raw material. The chemical composition of that glass, alkaline borosilicate glass (ABG), was reported earlier [6]. TRISO particles were mixed uniformly with ABG powder using vibration. The vibration was carried out in a graphite-tungsten die at different waste loadings: 10, 20 and 30 wt%. The mixtures were then hot-isostatic sintered at a pressure of 500 MPa and a temperature of 700 °C, as shown in Fig. 1a. The final samples were renamed according to their TRISO particle weight proportions: ABG-10, ABG-20 and ABG-30 corresponding to 10, 20 and 30 wt% waste loading. ABG-10 and ABG-30 are shown in Fig. 1b, c, respectively. Samples of 10 mm diameter and 2.75 mm thickness were prepared. The densities of samples were measured using the Archimedes method. The details of the sintering procedure are already well documented [5].

Characterisation

The interfacial bonding between the TRISO particles and ABG was investigated using a scanning electron microscope (SEM) by FEI/Philips (XL-30 FEG-SEM, Netherland) equipped with an Electron X-ray dispersive spectroscope (EDS). The samples were polished with diamond paste to 0.1 μm and coated with gold. The chemical compositions and possible contamination phases in the glass matrix before and after encapsulation were investigated using EDS. It was done in order to investigate the chemical properties of the glass and any possible carbon residue in the glass matrix that could be derived from the SiC layer. The contamination in ABG-10, ABG-20 and ABG-30 (such as SiC derived from TRISO particles) can be accurately quantified, which consequently can affect the bulk thermal diffusivity.

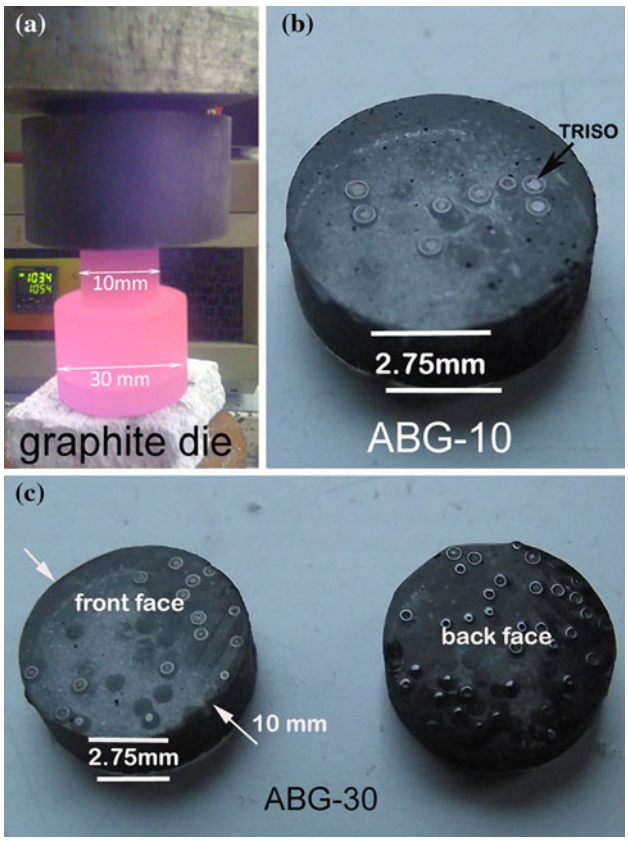

Fig. 1 **a** image shows tungsten–graphite die during hot-isostatic pressing. **b** Image shows ABG-10 bearing TRISO particles and **c** Image shows ABG-30 *front* and *back* faces

Laser flash analysis (LFA)

The measurement of thermal diffusivities was carried out using a Netzsch Micro-Flash 457 instrument. The front surface was uniformly heated by a pulse source of Nd:glass laser of spot size 1 mm, with a pulse duration of 0.3 ms, wavelength of 1064 nm and energy of 2.5 J [12]. The temperature at the back surface of the samples was measured using a liquid nitrogen-cooled photovoltaic Infra-Red

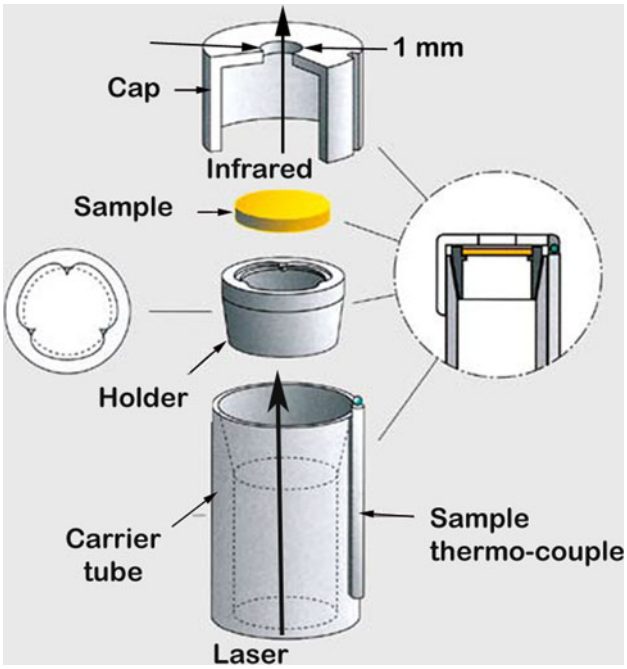

Fig. 2 Schematic of the sample holder fitted in LFA Netzsch Micro-Flash 457 [12]

(IR) thermocouple. A disc-shaped sample was coated with a graphite thin layer to improve the emissivity and it was mounted inside a SiC holder. The holder had an internal three-teeth ring located inside a sub-sector in order to minimize the heat conduction from the specimen to the holder, as shown in Fig. 2. The IR data collection time was set for a fixed time duration of 10 s. The device was calibrated with a standard graphite sample with less than 2 % deviation. The thermal diffusivities were measured at 50 °C. The temperature was measured from the sample thermocouple shown in Fig. 2. The IR beam collected through a hole fitted in a cap was placed over both the sample and the sample holder. The cap prevented the laser beam from impinging directly on the detector. This prevented damage to the IR detector as well as signal disturbance. The diameter of the hole in the cap was 1 mm [12]. The thermal diffusivity was calculated using Parker's model and the standard heat loss was corrected according to Cowan-fit plus pulse.

Modelling

The distribution of TRISO particles within a matrix was scanned using X-ray tomography on a Nikon Metris Custom Bay 225 kV X-ray instrument, fitted with a multi-metal anode target with an optimum spot size of 3 μm. During the analysis, the specimen was rotated by 360° and the projections were recorded on a 2 × 2 k PerkinElmer 16-bit, amorphous, silicon, flat-panel detector with approximately 200 pixel pitch. For the analysis, a copper X-ray target was used and the resolution was 37 μm for the specimen area within a diameter of 10 mm. The following settings were used for the analysis: scanning time 15 min, voltage 120 kV, current 60 μA, digital gain 1, number of frames 1000 and no filters.

Post-processing of the raw CT data included data reconstruction, using Nikon Metrolasis CT-Pro software (Metris XT 1.6), and data visualization, using Avizo standard software (VGS, version 7). All materials were segmented according to their greyscale values and labelled with four masks (ZrO_2 kernel, PyC, SiC and ABG); then, they were stored as 2D Tiff format images. It is important to mention that IPyC and a buffer, listed in Table 1, were merged into one mask called PyC. This simplification was feasible as it reduced the computational time and cost, and more importantly both layers have relatively similar thermal conductivity compared to that of SiC. In addition to this, both layers are closely attached to each other and they cannot be segmented away from each other.

The scanned data were imported into Simpleware software, converting the 2D Tiff format images into one 3D FE mesh. The same resolution (37 μm) was preserved during the conversion in order to capture all the detailed features of the SiC layer and generate a manageable INP format file (337 MB). The INP format file was imported into a commercial FE solver Abaqus Standard (Simulia, Providence, RI, USA).

Simulations were performed in Abaqus and the material properties were assigned for each mask at the temperature of 50 °C. 3D linear diffusion 4-noded (DC3D4) and 8-noded (DC3D8) elements have been employed. The number of elements was 14.7×10^6 and the number of nodes was 3.8×10^6. The resulting model had a very low count of distorted elements (6600) and therefore, it was considered as the perfect quality FE model.

Abaqus solves the Fourier law, with heat flow being proportional to the temperature gradient in one dimension as shown in Eq. 3:

$$q_x = k_x \frac{dT}{dx}, \tag{3}$$

where q_x is the average heat flux and k_x is the thermal conductivity in the x-direction.

To simulate the experimental setup, the same shape of the laser pulse was applied at the front face of the sample, whilst the response of temperature with time was measured on the rear face by selecting a nodal set of 1-mm-diameter circular area. The simulated laser pulse was developed in a way that identically matched the pattern of the LFA laser pulse. The convection heat loss and the radiation surface heat loss from the top and the circumferential edge surface were only considered because the heat loss from the rear face was fully captured and measured by the IR detector.

The steps for thermal loading and temperature recording at the rear face were created for a total period of 10 s over three transient time domains. This was done to allow the heat pulse to propagate through the whole sample and to collect sufficient data for the plot of half-rise time ($t_{1/2}$). The fixed increments were created in order to have greater control over time step size, which would also prevent the solution divergence. Additionally, each time step was restricted to have a maximum allowable temperature and emissivity change per increment of 1 °C and 0.1, respectively. The recording increment was 0.05 over 10 s of total time.

The input thermal properties of TRISO particle layers were obtained from Table 1. The thermal diffusivity of the ABG-0 sample (glass matrix without TRISO particles) was obtained by measuring it experimentally through LFA; it was found to be 0.411 $m^2\ s^{-1}$. The specific heat (C_p) was measured using a differential scanning calorimeter (DSC) instrument by Netzsch (STA 449 F1 Jupiter, Germany); it was found to be 0.8 kJ $kg^{-1}\ K^{-1}$. The specimen was heated at a rate of 10 °C min^{-1} and in air atmosphere. The device was calibrated with alumina standard; the standard deviation was 6 %. The density (ρ) was 1700 $kg.m^{-3}$ and it was obtained by the Archimedes method. The results of the above measurements were used in Eq. 1 in order to calculate the thermal conductivity of ABG-0, which was 0.77 W $m^{-1}\ K^{-1}$. These values were used as glass material properties in Abaqus software for consecutive samples ABG-10, ABG-20 and ABG-30. In the present study, the thermal conductivity of ABG-0 was lower than that of alumina borosilicate glass (1.10 W $m^{-1}\ K^{-1}$) as reported by Lima et al. [13]. The difference could be due to the air void content in our glass that occurred during the hot-isostatic sintering.

Results

The particles embedded in glass were investigated using Back Scattered Electrons (BSE) as shown in Fig. 3a; minor air voids were labelled in the matrix. A strong bonding between SiC layer and the glass was observed at the interface. EDS values were obtained at different points (Fig. 3a) to estimate the carbon content within the interface. Figure 3b shows the EDS pattern of the matrix before encapsulation and after encapsulation (labelled as X_1, X_2, X_3, X_4 and X_5). The EDS patterns show an increase of carbon content in the glass near the SiC layer. The initial carbon content in the glass was zero. Carbon contents in the specimen decreased from the maximum value in spot X_1 (SiC layer) to the lowest value in spot X_5.

The CT data scan of sample ABG-30 is displayed in Fig. 4a. The specimens (glass, SiC, pyrolytic carbon and

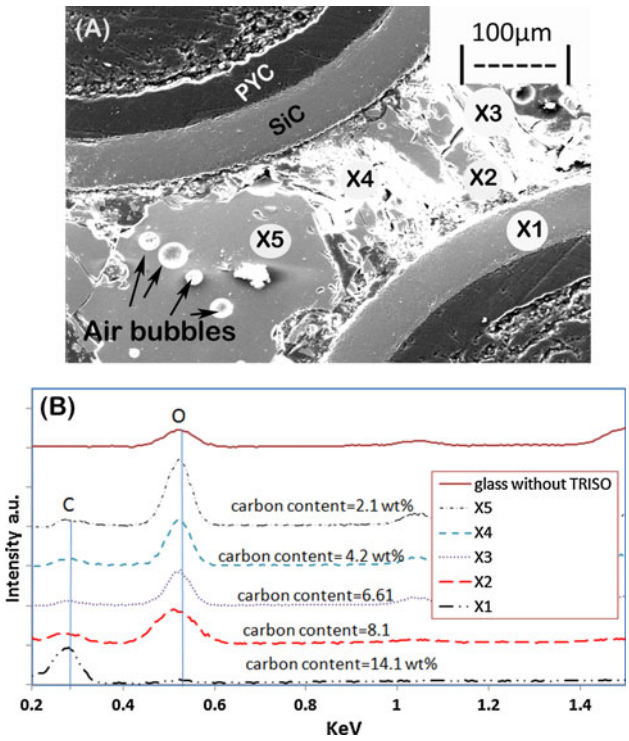

Fig. 3 **a** BSE micrograph of cross section TRISO particle, **b** EDS spectra of the glass (without TRISO) and after encapsulation at various spots as shown in **a**

ZrO_2) were segmented with 4 masks according to their greyscale values. A high magnification image of one TRISO particle in glass, displayed in Fig. 4b, shows that the phase contrasts were sufficient for the segmentation. Air voids were neglected to simplify the simulation and to reduce the number of FE, therefore allowing a workstation of 64 GB physical memory capacity to process the data. The segmented TRISO particles and glass are shown in Fig. 4c. The cross section of the specimen without glass matrix is shown in Fig. 4d; the red colour represents SiC, white represents PyC and blue represents the ZrO_2 kernel. It is worth noting that non-uniform distribution of particles was observed in all specimens. Consequently, this research demonstrates IBM as a powerful tool to provide precise particles' distribution, and also generates the most accurate model for the thermal heat transfer simulation.

A mesh size of 9.5×10^6 tetrahedral and 4.6×10^6 hexagonal elements was successfully generated using Simpleware software, as shown in Fig. 5a. This large number of elements was generated because 100 % resolution was implemented during the export of an INP format file from Simpleware software (no downsampling or rescaling from the original scan was performed). An attempt to reduce that large number of elements to a size of 5.5×10^6 tetrahedral and 1.2×10^6 hexagonal elements was carried out using the mesh growth option in

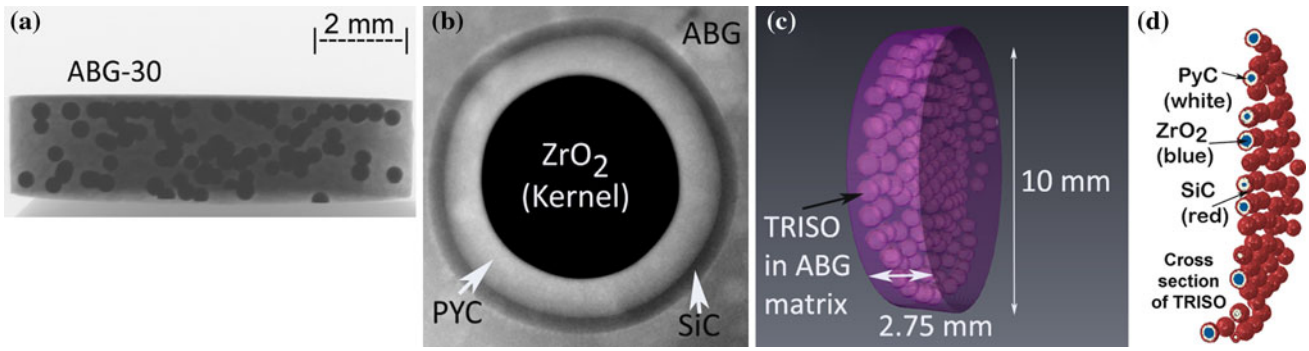

Fig. 4 **a** X-ray tomographic of ABG-30 (10 mm × 2.75 mm), **b** X-ray tomographic of one TRISO particle in glass, **c** rendered image with labelled ABG and TRISO particles, **d** rendered image of cross section of TRISO particles without glass. *Colour masks* are only available in the online paper version

Simpleware (32 × 32 × 32). The direction of the mesh growth was labelled in Fig. 5b.

However, the algorithm of mesh growth in Simpleware cannot be controlled through any parameter settings. Consequently, this can affect the material dimensions and the precise boundaries of the interface layer (SiC–glass). Therefore, the elements were switched back to their original size and further reductions were not conducted during the meshing process. Thus, no mesh growth was carried out during the mesh process. Air voids labelled in Fig. 3a were ignored to simplify the model and avoid high computation cost. The FE mesh size (14.1×10^6) was dramatically increased once elements which represent the air voids were included in the model. The void fraction was 5.1 vol% determined using material statistics in the Avizo programme.

The simulation was performed using Abaqus with the same parameters used in the LFA. The thermal loading procedure started with the preparation of three steps. Step 1 was to ramp the load up. Step 2 was to ramp the load down, which was achieved according to the signal amplitude identical to the LFA pulse shape, shown in Fig. 6. The final step 3 was to record the temperature changes with time, when the laser pulse was deactivated.

A laser pulse of 1-mm-diameter spot size was applied on the front surface as shown in Fig. 7a. The non-uniform temperature distribution is visible on the front face (Fig. 7b) and the back face (Fig. 7c) of the specimen. The temperature values were collected as average temperatures from a circular disc-shaped nodal set, instead of a single node set. Thus, simulating the response of the IR detector, the circular area (1 mm) is labelled in Fig. 7c. The normalised temperature (T_n) is expressed in Eq. 4:

$$T_n = \frac{(T - T_{min})}{(T_{max} - T_{min})} \quad (4)$$

T_{min} is the initial temperature condition of 50 °C and T_{max} is the maximum temperature rise. Therefore, the time

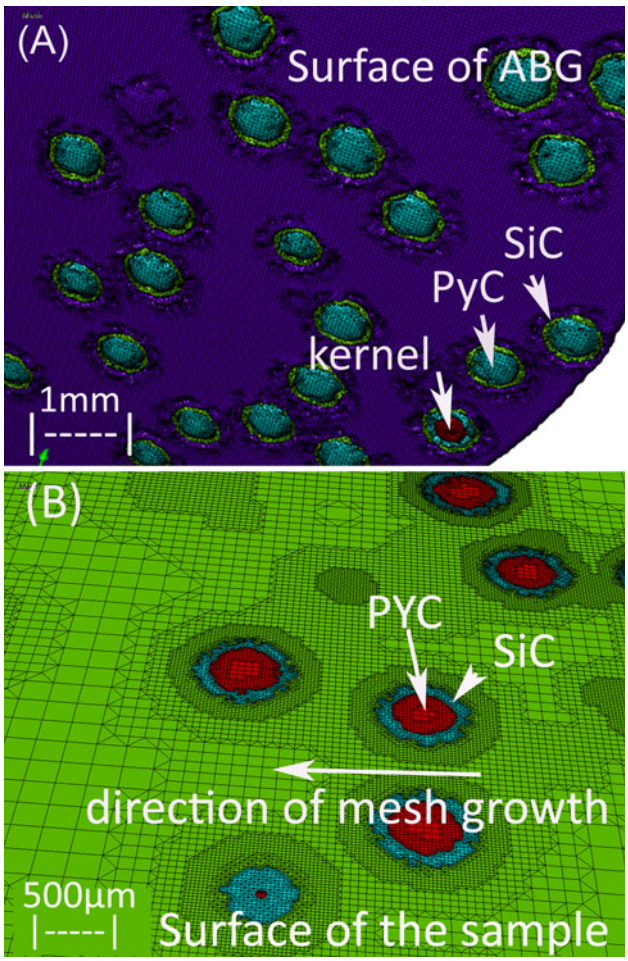

Fig. 5 **a** Rendered Image shows unchanged mesh size (14.1×10^6) of ABG surface. **b** rendered image shows a reduced mesh size (6.7×10^6) of ABG surface using mesh growth

for half-rise value $T_n = 0.5$ is located and labelled as $t_{1/2}$. The responses from ABG-10, ABG-20 and ABG-30 were recorded from a 1-mm-diameter circular disc-shaped nodal set as shown in Fig. 8a. The correlation of normalised temperature rise (T_n) was plotted with time as shown in

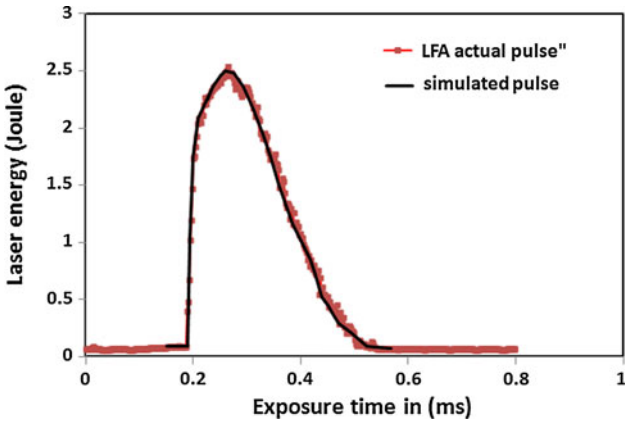

Fig. 6 Actual and simulated laser pulses, duration 0.3 ms

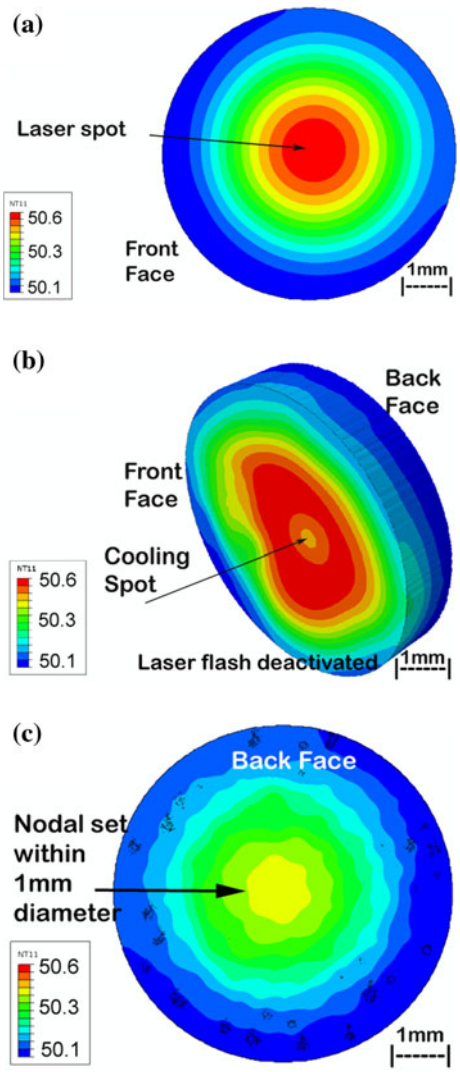

Fig. 7 **a** Post-processed contour plot shows thermal load spot on the specimen centre (step-1). **b** Post-processed contour plot shows the temperature gradient (step-2). **c** Post-processed contour plot shows the temperature gradient (step-3)

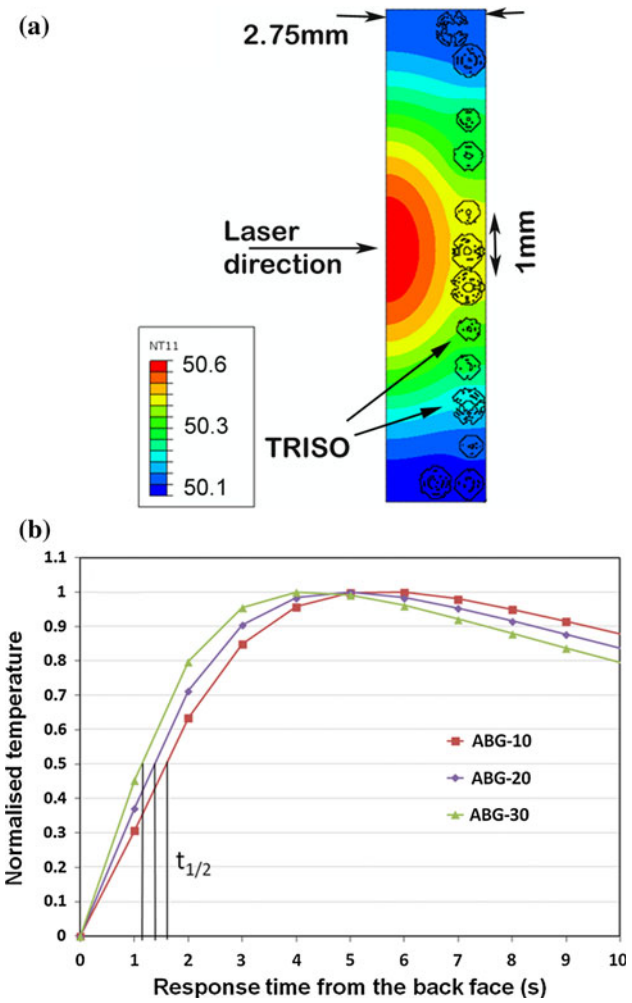

Fig. 8 **a** Post-processed contour plot shows the 1-mm-diameter *disc-shaped* nodal sets on the rear face of the sample. **b** Correlation of T_n with time collected from 1-mm-diameter *circular* nodal set

Fig. 8b. The thermal diffusivity was calculated using appropriate expression in Eq. 2 and is listed in Table 2. The radial heat losses from the boundaries were implemented as convection and radiation heat loss. The convection heat loss was selected as a film coefficient of 9.41 W m^{-2} K^{-1} and for radiation heat loss, an emissivity factor of 0.35 [14].

The calculated half-rise time values for ABG-10, ABG-20 and ABG-30 are listed in Table 2.

The time response from the rear face of the specimens obtained from the LFA instrument is displayed in Fig. 9. The thermal diffusivity values obtained from that time response using Eq. 2 are listed in Table 2.

The deviations($\pm$) of $t_{1/2}$ obtained from the experimental and modelled work are listed in Table 2. The modelled values collected from the 1-mm nodal set were in a close agreement with the experimental results and the error was in the range of 0.02–0.05 $\times$ 10^{-6} m^2 s^{-1}. Hence,

Table 2 Thermal diffusivity of ABG-0, ABG-10, ABG-20 and ABG-30 obtained from Abaqus software (α Model) for nodal set of 1 mm and from LFA (α Experimental)

Sample	$t_{1/2}$ Experimental (s)	$t_{1/2}$ Modelling (s)	α Experimental ($m^2\ s^{-1}$ x 10^{-6})	α Modelling ($m^2\ s^{-1}$ x 10^{-6})
ABG-0	2.55 ± 0.10	–	0.411 ± 0.025	–
ABG-10	1.65 ± 0.05	1.70	0.636 ± 0.015	0.617
ABG-20	1.42 ± 0.05	1.32	0.739 ± 0.025	0.79
ABG-30	1.13 ± 0.05	1.11	0.92 ± 0.021	0.94

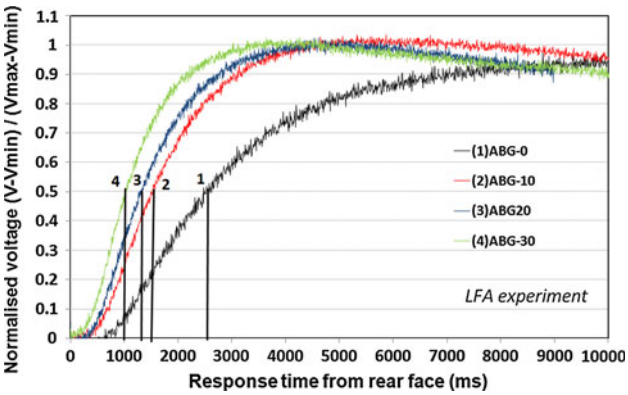

Fig. 9 Graph shows the temperature change with time from rear face of ABG-0, ABG-10, ABG-20 and ABG-30 obtained from the LFA instrument (corresponding to T_n)

the 1-mm nodal set data validated the experimental values with a deviation of less than 5 %, which was set as a limit in a previous study for the validation of the experimental work using modelling [15]. In order to monitor the radial thermal diffusivity, temperatures from the node sets located at radial diameters of 6 and 8 mm were also measured as shown in Fig. 10a. The time response was plotted as shown in Fig. 10b and c, in order to obtain $t_{1/2}$ and consequently the relevant thermal diffusivity. This can provide inspiration to perform radial off-centre experimental work in the future in order to validate the simulation work.

The simulated thermal diffusivity values (α Model) obtained from 1-, 6- and 8-mm nodal sets were plotted in Fig. 11. This was done in order to observe the radial off-centre thermal diffusivity trend for all specimens.

Discussion

A glass matrix was developed to immobilize surrogate TRISO particles. The thermal diffusivity of the matrix bearing TRISO particles was measured experimentally using LFA and simulated using IBM and FE solver. The IBM technique was selected in order to obtain the nearest geometry of glass matrix samples bearing different proportions of TRISO particles. The layers in some of the TRISO particles experience geometry changes during FBCVD. This resulted in creation of particles which are not exactly spherical in shape. These changes were not evident in the 2D image (Fig. 4b), a but distortion can clearly be observed in the BSE image of particles in Fig. 12. Thus, considering TRISO particles as a perfect sphere would not reflect the reality and may give inaccurate results for the thermal simulation of the repository at large. In addition, the spent TRISO particles' performance in the repository requires evaluation of heat flow at the microscale. Thus, 3D thermal modelling of TRISO particles was a crucial part of the whole analysis and IBM presents the closest possible 3D model.

In this study, a 3D model has been solved using finite element solver. High resolution of the scan data has been taken in order to analyse 3D model, using IBM, to match the results with the experimental data of LFA. The uncertainty in measurement of the thermal diffusivity depends on the resolution of the CT data used during the modelling process. Thus, the critical parameter is to obtain high resolution data from X-ray CT and apply exact heat convection and radiation loss during the modelling process. However, TRISO particles were embedded inside ABG using hot-isostatic sintering and therefore, air voids were unavoidable at the microscale level. The air voids smaller than 37 μm were not captured using X-rays tomography scan; thus, they could not be taken into consideration during IBM. The air voids bigger than 37 μm were successfully captured, but they were replaced by glass mask using Simpleware software. Thus, they were neglected as air voids for ease of computation. It allowed us to avoid additional tetrahedral elements forming irregular void shapes and to maintain uniformity in the glass mask. At the same time, it had an impact on the reduction of the actual glass thermal diffusivity. The simulation of the model without air voids may have higher thermal diffusivity (positive deviation) than the experimental results. A similar positive deviation was noted by a previous study which investigated 11 % porosity of air voids in a carbon fibre matrix [16]. Therefore, α-Modelling obtained through simulation was higher than the values acquired through experiments (Table 2).

Another factor which is contributing to the difference between the experimental and the modelled thermal

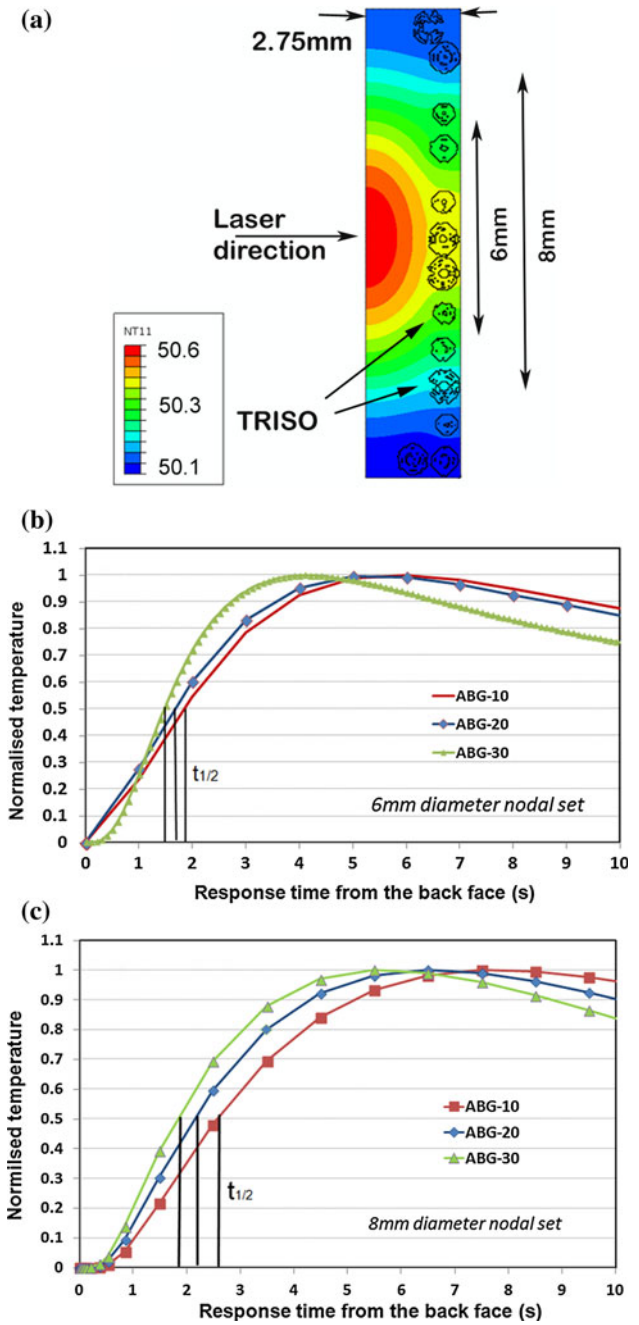

Fig. 10 **a** Post-processed contour plot shows the diameter of different disc-shaped nodal sets on the rear face of the sample. **b** Correlation of T_n with time from 6-mm-diameter *circular* nodal sets. **c** Correlation of T_n with time from 8-mm-diameter *circular* nodal sets

diffusivity is the contamination of glass with carbon derived from SiC layer during encapsulation. This may result in a lower value of α-Modelling than α-Experimental and consequently a negative deviation. Furthermore, there is considerable noise in the LFA time response graph shown in Fig. 9. Although radial heat loss due to the sample's contact with the three teeth of the sample holder shown in Fig. 2 was not considered, it was nevertheless

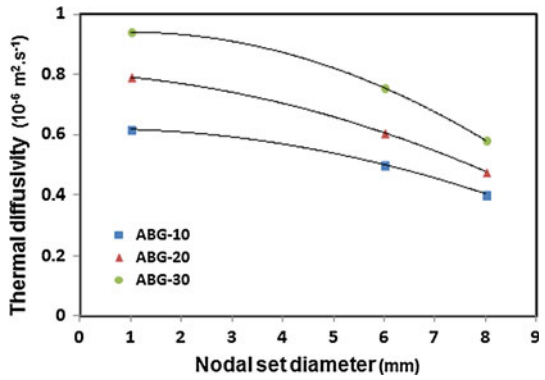

Fig. 11 Graph shows the correlation of thermal diffusivity obtained from *circular* nodal sets (diameters 1, 6, 8 mm) on the rear face (*curves* only to guide the eyes)

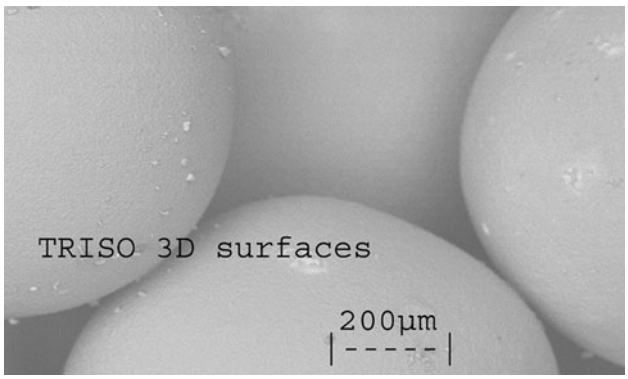

Fig. 12 BSE image shows non-spherical TRISO particles before encapsulation in glass

assumed to be insignificant in measurements taken at a low temperature (50 °C). In a previous study, the heat loss was estimated to be approximately 0.12 and 0.23 % of the total energy input to the specimen due to convection heat loss and radiation heat loss, respectively [14]. The measurements assumed that the wall was maintained at 52.5 °C for 1 s [14].

From materials' point of view, strong interfacial bonding between the TRISO particles and glass was experienced during cutting, grinding and polishing of samples (displayed in Fig. 1b, c). This clearly shows that a rigid matrix can be obtained from the process of hot-isostatic sintering [1].

Both measurements confirmed that the high thermal conductivity of SiC layer (168 W m^{-1} K^{-1}) increased the bulk thermal diffusivity. However, the results confirmed that including 30 wt% of TRISO particles in glass increased its bulk thermal diffusivity by twofold. Moreover, it is not clear yet whether such values of thermal diffusivity are sufficient for dissipating the decay heat from spent radioactive TRISO particles to the repository. It is critical that thermal property mismatch will form cracks or

hot spots at the interface due to differences in thermal expansion coefficient. However, that could be accurately simulated in a future research by imposing heat-generating kernels.

The radial thermal diffusivity plotted in Fig. 11 shows the trend of these values with their corresponding circular disc-based nodal set diameter, which can also be linked with heat-generating kernels in a future research. This radial thermal diffusivity from the waste form can be correlated with the decay time of the heat-generated radioactive waste.

Conclusion

The main advantage of using the IBM technique is to rule out the effect of non-uniform distribution of TRISO particles embedded in glass matrix. The thermal diffusivities of ABG-10, ABG-20 and ABG-30 were measured experimentally using LFA and validated by simulating similar parameters using Abaqus software. The deviations between the correspondent values obtained from both methods were less than 5 %.

The study demonstrates that surrogate TRISO particles can be successfully immobilized in glass, which enhanced its thermal diffusivity. Despite the fact that the TRISO particles have high thermal conductivity due to their SiC layer, the encapsulation has only approximately doubled the thermal diffusivity compared with its initial values. IBM has proven to be a powerful tool to simulate the fine structure of specimens, and the accuracy of implementing the heat load was the key parameter of this research. Full resolution (no downsampling from the original CT data) of all models was implemented in order to obtain the close agreement between values obtained from both experimental and modelling methods. Deviations in the values obtained from both methods were mainly due to neglecting the air voids, carbon content and fluctuation in the experimental time responses. Future work can be focused on the effect of forming hot spots at interface of TRISO/glass due to heat generation from the kernel. The simulation method could measure the heat flow towards the circumferential boundary with decay time of the fission products in the kernel.

Acknowledgements The authors thank the material science centre for performing the LFA work and the EPSRC for the grant that funded the project (EP/F007906/1). The authors would like to acknowledge the role of Mrs. Ewa Skibicka for editing the tautology of this article and the Commonwealth Academic Research Trust (CART) for arranging TRISO particles for this research.

References

1. Bari K, Lowe T, Abram TJ (2012) Interaction of embedded tri-isotropic fuel particles with melt of alkaline borosilicate glass. Int J Appl Glass Sci 3(3):254–262
2. López-Honorato E, Chiritescu C, Xiao P, Cahill G, Marsh DG, Abram TJ (2008) Thermal conductivity mapping of pyrolytic carbon and silicon carbide coatings on simulated fuel particles by time-domain thermoreflectance. J Nucl Mater 378(1):35–39
3. Hasselman DPH, Johnson LF, Syed R, Taylor MP, Chyungi K (1987) Heat conduction characteristics of a carbon-fibre-reinforced lithia-alumino-silicate glass-ceramic. J Mater Sci 22(2):701–709. doi:10.1007/bf01160791
4. Parker WJ, Jenkins CP, Butler CP, Abbott GL (1961) A flash method of determining thermal diffusivity, heat capacity and thermal conductivity. J Appl Phys 32(9):1679–1684
5. Bari K, Abram TJ (2011) Microstructure characterization of simulated tri-isotropic particles embedded in alkaline borosilicate glass. Int J Appl Glass Sci 2(4):334–342
6. Bari K, Abram TJ, Lowe T, Cernik RJ, López-Honorato E (2013) The chemical durability of glass and graphite–glass composite doped with cesium oxide. J Nucl Mater 432(1–3):529–538
7. Jantzen CM, Bickford DF, Karraker DG (1983) Time–temperature transformation kinetics in srl waste glass. In: Conference proceeding of 2nd international symposium on ceramics in Nuclear waste Management, Ohio, USA
8. Gdowski GE, Wolery TJ, Rosenberg ND (2002) Waste Package Environment for the Yucca Mountain Site Characterization Project. In: MRS Proceedings, USA. doi:10.1557/PROC-713-JJ1.3
9. Tix C (1996) On the behaviour of cavities in a viscoplastic medium with application to underground repositories of radioactive waste in salt domes. J Phys D Appl Phys 29(4):1100–1110
10. Avila R, Cervantes J, Estrada-Gasca C (2000) Transient thermal response in nuclear waste repositories. Nucl Eng Des 198(3):307–316
11. Kercher A, Hunn J (2005) Results from ORNL Characterization of ZrO2-500-AK2-Surrogate TRISO particles. Oak Ridge National Laboratory, USA
12. Netzsch (2012) Technical, analyzing and testing manual/LFA 457 MicroFlash. www.netzsch-thermal-analysis.com. Accessed 12 oct 2012
13. Lima MM, Monteiro RC, Graça MPF, FerreiradaSilva MG (2012) Structural, electrical and thermal properties of borosilicate glass–alumina composites. J Alloy Compd 538:66–72
14. Sheikh MA, Taylor SC, Hayhurst DR, Taylor R (2000) Measurement of thermal diffusivity of isotropic materials using a laser flash method and its validation by finite element analysis. J Phys D Appl Phys 33(12):1536
15. Donaldson A, Taylor R (1975) Thermal diffusivity measurement by a radial heat flow method. J Appl Phys 46(10):4584
16. Farooqi JK, Sheikh MA (2006) Finite element modeling of thermal transport in ceramic matrix composites. Comput Mater Sci 37(3):361–373. doi:10.1115/1.2193547